An experimental and theoretical high temperature kinetic study of the thermal unimolecular dissociation of fluoroethane

Binod R. Giri,†[a] John. H. Kiefer,[b] Hui Xu,‡[b] Stephen J. Klippenstein[a] and Robert S. Tranter*[a]

Received 14th May 2008, Accepted 3rd July 2008
First published as an Advance Article on the web 10th September 2008
DOI: 10.1039/b808168a

The thermal dissociation of fluoroethane has been studied using shock tube (ST)/time-of-flight mass spectrometry (TOF-MS) at 500 and 1200 Torr over the temperature range 1200–1550 K. The ST/TOF-MS experiments confirm that elimination of HF is the only reaction channel and rate coefficients for this reaction were extracted from concentration/time profiles derived from the mass spectra. Results from a novel diaphragmless shock tube coupled to the TOF-MS are also presented and demonstrate the unique ability of this apparatus to generate sufficiently reproducible shock waves that signal averaging can be performed over multiple experiments; something that is not possible with a conventional shock tube. The dissociation is also studied with *ab initio* transition state theory based master equation simulations. A modest increase in the calculated barrier height (*i.e.*, by 1 kcal mol^{-1}) yields predicted high pressure rate coefficients that are in good agreement with the existing literature data. The present pressure dependent observations are accurately reproduced for a downwards energy transfer for neon at 1200 to 1500 K of $\sim$270 cm^{-1}, which is somewhat smaller than that found in previous studies on fluorinated ethanes with the same bath gases.

Introduction

Elimination of hydrogen fluoride from fluorinated ethanes has been extensively studied at conditions close to the high pressure limit, see ref. 1 and 2 and references therein. Generally, good agreement with k_∞ derived from theoretical calculations is found. These studies indicate that the elimination of HF proceeds *via* a four centered transition state.

Until recently, no experimental data concerning HF elimination from fluorinated ethanes in the high temperature fall off region were available. A high temperature shock tube/laser schlieren (ST/LS) study of 1,1,1-trifluoroethane (TFE) gave the surprising result of deep fall off from k_∞ but little pressure dependence.[1] Based on observations of double relaxation in the same study and the inability of standard RRKM models to simulate the data the authors tentatively concluded that the dissociation of TFE at high temperatures was non-statistical in nature. Very recently, support for the ST/LS results was obtained from a new shock tube/time-of-flight mass spectrometer (ST/TOF-MS) study.[2] The laser schlieren studies also prompted theoretical investigations,[3,4] the results of which question the source of the apparent non-RRKM behavior in the ST/LS experiments.

Non-RRKM behavior is very rare although much anticipated, see ref. 1 and references therein. Consequently, investigation of other fluorinated ethanes, at conditions similar to the ST/LS TFE studies, may yield better understanding of vibrational relaxation and HF elimination. Additionally, a more extensive dataset describing the fall off behavior of HF elimination from fluoroethanes will be gained. To date we have studied vibrational relaxation and dissociation of TFE,[1] 1,1-difluoroethane[5] and ethane itself[6] in the high temperature fall off region. 1-Fluoroethane, FE, concludes the series of fluorinated alkanes where the substituents are on a single carbon atom.

We have previously applied both ST/LS and ST/TOF-MS to the study of TFE[2] and vinyl fluoride,[5] the main decomposition product of DFE. The combination of these two techniques allows coverage of a much wider experimental range for the dissociation reaction than is possible by either method alone.[5] ST/LS appears to be uniquely suited to observation of vibrational relaxation at high temperatures and the ST/TOF-MS technique provides confirmation of rate and mechanism through direct identification of reaction products.

The LS technique effectively measures density gradients, $d\rho/dx$, and these are proportional to the rate, r, through the heat of reaction, ΔH, with a usually small reduction from expansion through any increase in mole number, ΔN, as in eqn (1).

$$\frac{d\rho}{dx} = \frac{\rho \sum r(\Delta H - C_p T \Delta N)}{\rho_0 u(C_p T/M - C_v v^2/R)} \quad (1)$$

Here, the remaining quantities are just molecular heat capacities or incident shock parameters, which are easily obtained from measurements or calculations.[7] The value of the

[a] *Chemical Sciences and Engineering Division, Argonne National Laboratory, 9700 South Cass Avenue, Argonne, IL 60439-4831, USA. E-mail: tranter@anl.gov*
[b] *Department of Chemical Engineering, University of Illinois at Chicago, Chicago, IL-60607, USA*
† Current address: Department of Chemistry, Acadia University, Wolfville, Nova Scotia, Canada.
‡ Current address: Cummins Inc., Cummins Technical Center, 1900 McKinley Ave, Columbus, IN-47201, USA.

expression $C_pT\Delta N$ is typically of the order 10–15 kcal mol^{-1}. The literature values of $\Delta H_{f,298}$ for FE are −65.8 kcal mol^{-1},[8] −66.5 kcal mol^{-1},[9] −65.1 kcal mol^{-1}[10] and −62.9 kcal mol^{-1}[11] and so the dissociation of FE is endothermic by, at most, just 13.7 kcal mol^{-1}. Thus, for the dissociation of FE, very small to vanishing density gradients will be produced, effectively rendering the technique blind to this reaction. Hence, here we present only ST/TOF-MS measurements of HF elimination and confine ST/LS to measurements of vibrational relaxation.

The majority of the literature data for dissociation of FE are below 1000 K. Day and Trotman-Dickenson[12] studied the reaction in a static reactor over the temperature range 684–739 K and pressures of 0.7–216 Torr. They observed virtually no pressure dependence and obtained Arrhenius parameters, log A = 13.31 and E_a = 58.2 kcal mol^{-1}. In subsequent work, Kerr and Timlin[13] employed a similar technique using identical conditions to that of Day and Trotman-Dickenson, and obtained excellent agreement with the earlier results. Sianesi *et al.*[14] observed pyrolysis in a conventional flow system (T = 843–923 K, P = 1 atm) and reported a rate coefficient expression for FE dissociation that had a pre-exponential factor which was a factor of 13 greater than that of Kerr and Timlin and an activation energy which was 4.4 kcal mol^{-1} larger. Rate coefficients calculated from Sinaesi *et al.*'s expression are however in good agreement with the extrapolated lower temperature data from Kerr and Timlin. A similar flow reactor study by Dastoor and Emovon,[15] however, reported rate coefficients for T = 793–873 K that were more than an order of magnitude slower than the earlier studies. However, as noted by Kerr and Timlin,[13] the pre-exponential factor (log A = 12.16) appears to be too low to account for a reasonable change in the entropy of activation for such HF elimination.

Above 1000 K, the only literature data are two single-pulse shock tube studies.[16,17] Okada *et al.*[16] studied FE dissociation at P = 2500–8700 Torr and T = 996–1137 K using the relative rate method and deduced a high pressure limiting rate expression: $k_\infty(T) = 10^{13.65\pm0.20}\exp(-59.5 \pm 1.0 \text{ kcal mol}^{-1}/RT)$ s^{-1}. Cadman *et al.*[17] also used the single pulse shock tube method and their results for T = 1275–1659 K and $P \approx$ 800 Torr indicate a small fall off from the likely high pressure limit of Okada *et al.* However, the reliability of Cadman *et al.*'s data for HF eliminations has been seriously questioned[16,18] and it appears likely that agreement with other datasets may be fortuitous.

Experimental

ST/LS

The shock tube used in the LS experiments has a 4 ft long driver section of 4 in id connected to a 10 ft driven section of 2.5 in id, whose detailed layout has been fully described.[19] The ST/LS diagnostics and software have also been described previously.[7,20–22] As before,[19] velocities were set by interpolation of four intervals calculated from measured times centered about the LS beam. On the basis of extensive experience, the uncertainty in velocity is estimated as ±0.2%, corresponding to a temperature error of less than ±0.5%, here amounting to the order of ±10 K.

To produce the very weak shocks necessary for observation of the fast relaxation found in these fluorides, a slow flow of driver gas was achieved by introducing various converging/diverging nozzles of different throat diameters at the diaphragm. The experiments all used Mylar diaphragms of 0.001–0.005 in thickness, burst spontaneously with helium. Molar refractivities used in the calculation of the density gradient from the measured angular deflection were 11.38 for fluoroethane[23] and 6.367 for Kr.[24] These were taken as constant throughout the decomposition; an excellent approximation for such species.

ST/TOF-MS and DFST/TOF-MS

The ST/TOF-MS and differentially pumped molecular beam sampling system that couples the shock tube and TOF-MS have been extensively described elsewhere.[2,25] The shock tube consists of a 23 in long, 7.7 in id driver section and 23 ft. long driven section that reduces from 2.8 in id to 2.5 in id as it enters the sampling system.[25] Pressure transducers are located close to the end wall of the driven section and the shock velocities and hence post shock conditions are obtained in a similar manner to the ST/LS experiments with similar uncertainties.

Recently, the driver section of the shock tube has been modified to create a diaphragmless shock tube, DFST which is fully described elsewhere.[26] Essentially, the diaphragm has been replaced by a novel, fast acting valve mounted inside the driver section and this is shown schematically in Fig. 1. Initially the interior of the bellows is pressurized causing the bellows to expand and push the seal plate into the throat of the driven section thereby separating the driver and driven sections. This is the configuration shown in Fig. 1. The two sections of the shock tube can now be filled to the desired pressures and then fired by rapidly venting the bellows causing them to collapse and draw the seal plate out of the driven section. The DFST has several advantages that are discussed elsewhere.[26] Of particular relevance to the current study is that very reproducible reaction conditions can be achieved[26] for separate experiments with identical loading conditions. This reproducibility gives rise to the possibility of signal averaging over multiple experiments to improve signal quality. In the current work, both the diaphragmed shock tube and the diaphragmless apparatus were used and from hereon DST

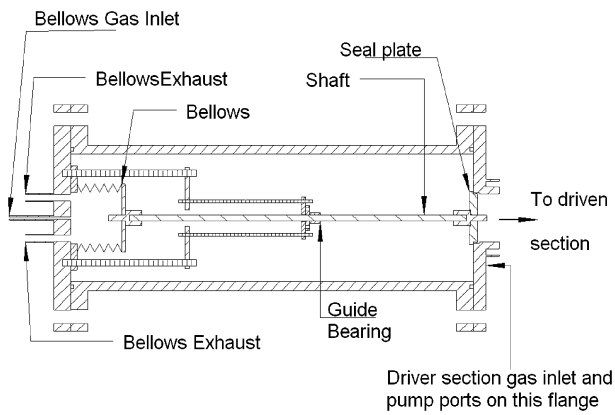

Fig. 1 Schematic of the diaphragmless driver section of the DFST.

will be used to refer to the shock tube operated with diaphragms and ST to refer to both DST and DFST.

Unlike the ST/LS experiments, which are conducted behind the incident shock waves, the ST/TOF-MS experiments are performed behind the reflected shock. Following reflection of the shock wave from the endwall, a thermal boundary layer grows into the shock heated zone. Sampling from this layer is avoided by the use of a differentially pumped molecular beam system; the first stage of which is a 0.4 mm diameter orifice in the driven section endwall.[25] Gases flow continuously from the shock tube into the ion source of the reflectron mass spectrometer where ion packets are generated by electron impact ionization (30 eV). To produce well defined ion packets the electron beam is pulsed in and out of the ion source and this is synchronized with the draw out pulse used to gate ion packets into the TOF-MS for analysis.[25] The ionization pulse has a duration of 0.4 μs and ion packets are injected every 9.52 μs to obtain sufficient temporal resolution for determining the initial rate of reaction. The pressure in the ion source increases during the course of an experiment and the subsequent change in ion signals is accounted for with a non-reactive internal standard,[25] here argon. Both pre-shock and post-shock data are acquired and in-house software is used to interpret the mass spectra and create concentration/time profiles for the species of interest.

In ST/TOF-MS experiments it is not uncommon to observe peaks of greatly different sizes in the mass spectra which often force the sensitivity of the detector to be reduced to avoid saturation of the detector.[2] Consequently, the measurement of species with small peaks can be impaired. With the DST/TOF-MS each experiment has to be considered unique[2,26] and techniques such as signal averaging cannot be applied. However, with the DFST/TOF-MS, experiments performed with identical loading conditions in the shock tube produce sufficiently similar post shock conditions that variations are within the experimental error, and the results can be considered near identical.[26] Thus, as will be demonstrated, mass spectra from several experiments obtained from DFST/TOF-MS measurements can be averaged improving signal/noise, S/N, and the shapes of small peaks and reducing the scatter in concentration/time plots derived from the mass spectra.

Regent mixtures

All reaction mixtures were prepared manometrically in 50 L glass vessels. The mixtures were homogenized either through stirring (ST/LS) or diffusion overnight (ST/TOF-MS) prior to use. For both experiments fluoroethane (97 + %) was obtained from Synquest Laboratories. ST/LS mixtures contained 10 or 20% FE diluted in krypton (Spectra Gases excimer grade). The ST/TOF-MS reaction mixtures were, 1–4% FE, 1.5–6% argon (Linde 99.999%) diluted in neon (Linde 99.999%).

Theoretical calculations

The geometric structures and rovibrational properties of the reactants, products, and transition state for the dissociation of C_2H_5F into C_2H_4 + HF were studied with a variety of methods. Initial explorations were performed with density functional theory employing the Becke-3 Lee-Yang Parr (B3LYP)[27] functional and the 6-31G* and 6-311 + + G(d,p) basis sets.[28] The properties of the saddle point and products were further explored with second order perturbation theory (PT2)[29] employing a 4-electron 4-orbital complete active space (CAS). The active space consisted of the orbitals correlating with the HF bonding and antibonding orbitals and the C_2H_4 π and π* orbitals. Dunning's correlation consistent basis sets[30] up to cc-pvqz were employed in these CASPT2 calculations. Finally, the properties of the stationary points were examined with quadratic configuration interaction calculations with perturbative inclusion of triple excitations (QCISD(T)).[31] The largest basis set employed for these QCISD(T) calculations was the cc-pvtz basis set. The GAUSSIAN98[32] quantum chemistry package was used for all the B3LYP calculations, while the remaining calculations were performed with the MOLPRO[33] package.

There are only modest variations in the optimized structures and vibrational frequencies with quantum chemical method. The imaginary frequency shows the largest variation, with predicted values of 1965, 1977, 1927, and 1711 for the QCISD(T)/cc-pvtz, CASPT2/cc-pvtz, CASPT2/cc-pvqz, and B3LYP/6-311 + + G(d,p) calculations respectively. The variations in the remaining transition state frequencies yield variations of 20% or less in the predicted rate coefficients for temperatures in the 1000 to 2000 K regime.

Larger basis sets (up to cc-pvqz or aug-cc-pvqz) were employed in QCISD(T) single point calculations at the QCISD(T)/cc-pvtz, the B3LYP/6-311 + + G(d,p), and various of the CASPT2 optimized geometries. These QCISD(T)/cc-pvtz and QCISD(T)/cc-pvqz energies were extrapolated to the complete basis set (CBS) limit as in our prior studies.[34] Due in large part to the sharp nature of the barrier, there is little dependence of the barrier height on optimization method, with variations of less than 0.2 kcal mol^{-1} in the barrier height predicted for the different geometries. The basis set extrapolations based on the cc-pvnz and aug-cc-pvnz series yielded essentially identical results (differing by only 0.02) kcal mol^{-1}. This modest discrepancy suggests that the basis set extrapolation, which amounts to a lowering of the barrier height by ~0.4 kcal mol^{-1} from the cc-pvqz values, should be quite accurate.

The minimum energy path (MEP) was followed at the CASPT2/aug-cc-pvdz level with POLYRATE[35] coupled to a modified version of GAUSSRATE[36] that allowed for the direct use of the MOLPRO quantum chemistry software. This procedure also produced projected vibrational frequencies along the path. Higher level QCISD(T)/CBS energies were also obtained along the CASPT2/aug-cc-pvdz MEP. The latter energies, relative to the saddlepoint energy, were found to be essentially identical to those from the CASPT2/aug-cc-pvdz MEP. The CASPT2/aug-cc-pvdz properties along the MEP were employed in variational transition state theory calculations, yielding a nearly temperature independent reduction in the rate by 25% for temperatures in the 1000 to 2000 K range.

The effect of tunneling was examined with both one-dimensional Eckart corrections and with the small curvature tunneling formalism of Truhlar and coworkers.[37,38] These two methods were found to yield quantitatively similar tunneling corrections for temperatures in the 600 to 2000 K range. At

1000 K, tunneling increases the rate by a factor of 1.4, this factor reduces to 1.1 by 2000 K. For computational reasons, the one-dimensional Eckart tunneling correction was employed in the final temperature and pressure dependent calculations.

Master equation simulations of the temperature and pressure dependent kinetics were performed as described elsewhere.[39,40] The collision rate for collisions with neon was calculated from Lennard-Jones potentials. A single exponential-down model was employed for the energy transfer function. The average downwards energy transfer, $\langle \Delta E \rangle_{down}$, was taken to increase with temperature according to the form: 150 $(T/298)^n$ cm^{-1}. This form was chosen in analogy with our findings for a number of other reactions[40] and the specific values employed are based on a fit to experiment as discussed below. The internal rotor in ethyl fluoride was treated as a hindered rotor employing a Pitzer–Gwinn approximation.[41]

Results and discussion

Relaxation

In previous work on 1,1,1-trifluoroethane,[1] 1,1-difluroethane[5] and ethane[6] vibrational relaxation could be resolved in ST/LS experiments. For TFE and ethane double relaxation was observed with a fast initial process being followed by a slower secondary one that preceded dissociation. For completeness we attempted to study vibrational relaxation in fluoroethane. Unfortunately, although indications of vibrational relaxation were observed, the process was simply too fast to be clearly resolved preventing reliable data from being obtained. Consequently, no results from the vibrational relaxation experiments will be presented.

Dissociation

An example of the raw mass spectra and timing signals used to control the injections of ion–ion packets into the TOF-MS are shown in Fig. 2 with the regions corresponding to before and after reflection of the incident shock wave indicated. The increase in signal at approximately 350 μs is due to the increasing pressure in the ion source following reflection of the shock wave and in conjunction with concentration profiles is used to locate the onset of reaction, t_0.[25] The mass spectra for unreacted FE show a dominant peak at m/z = 47 and a minor peak at m/z = 48, the parent ion, which is about 10% the height of the m/z = 47 peak. Additionally, peaks at m/z = 33 (25% of m/z = 47) and m/z = 28 (10% of m/z = 47) are found along with several minor peaks. These observations are in good agreement with the literature MS for FE.[42] Fig. 3 shows a segment, from Fig. 2, 180 μs after the occurrence of the reflected shock wave, and a number of additional peaks that correspond to the reaction product ethylene and its fragments (m/z = 28, 27, 26). An additional peak at m/z = 20 is observed which could correspond to HF. However, the mass resolution of the current instrument HF is not sufficient to distinguish between HF and the bath gas neon. The formation of neon ions is minimized by using an ionization energy of 30 eV and the presence of HF is inferred through the increase in the m/z = 20 signal that occurs simultaneously

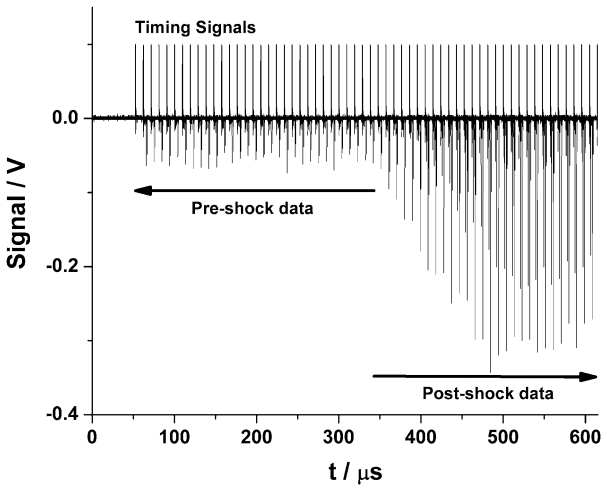

Fig. 2 Raw data obtained at an ionization cycle of 105 kHz from a ST/TOF-MS experiment, P_5 = 1262 Torr, T_5 = 1425 K. The downward spikes represent the mass spectra and show pre-shock as well as the post-shock data. The increase in signal intensity at 350 μs is discussed in the text. The upward spikes show the timing signals used to gate deflect the electron beam and gate the ion packets in the TOF-MS.

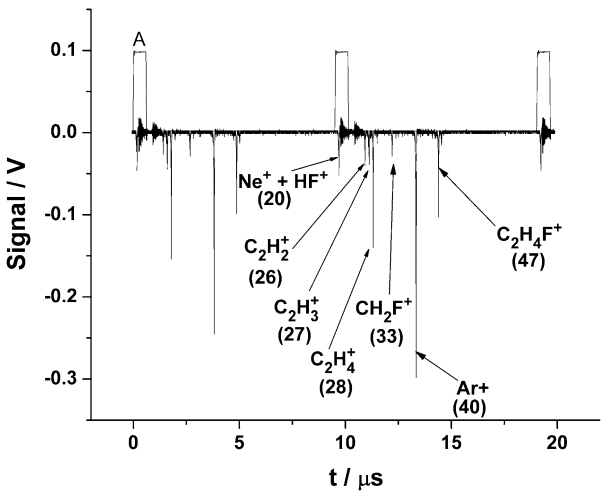

Fig. 3 A 20 μs time segment from Fig. 2 180 μs after formation of the reflected shock wave which defines the start of reaction. Ions are generated while the timing pulses are high and injected when the pulse goes low. The labeled peaks are associated with the pulse labeled, A, and the flight times are measured from the falling edge of this pulse. The unlabelled peaks belong to a prior pulse.

with the appearance of m/z = 28 and by comparison with experiments where the temperature is too low to dissociate FE. The peak areas in the mass spectrum are directly proportional to concentration and by integrating the peak areas for each m/z of interest in every mass spectrum and scaling by the argon peak area[2,25] concentration/time plots for each species are obtained, Fig. 4. Fragmentation of FE in the ion source generates small amounts of m/z = 28, 27 and 26 and this is accounted for in determining the C_2H_4 concentration. Initial estimates of the HF elimination rate coefficient for each experiment are obtained directly from the concentration/time

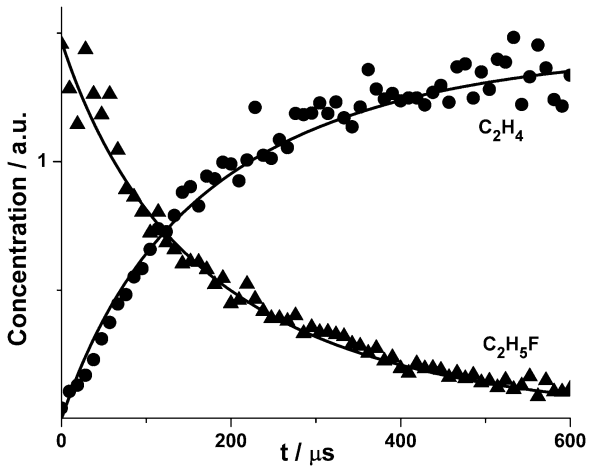

Fig. 4 Concentration/time plot for the dissociation of FE. Points are experimental data and the solid lines represent the results of simulations used to extract the initial rate coefficients and account for non-isothermal effects.

profiles assuming first order kinetics. To account for temperature changes during reaction, which are small due to the low endothermicity of the 1,2-HF elimination from FE, the estimated rate coefficients are refined through simulation.[2] The mass spectra show no evidence of reaction paths other than HF elimination and thus the model consists solely of a single reaction for 1,2 elimination.

In the current work the portion of the concentration/time profiles that correspond to gases sampled from behind the reflected shock wave, *e.g.* Fig. 4, are quite well defined. However, prior to formation of the reflected shock wave the pressure in the driven section of the shock tube is low, which results in a low density in the TOF-MS ion source and the production of few ions. Consequently, at early times the peaks in the mass spectra are poorly formed and susceptible to random fluctuations in area. This results in an increased scatter in the early portions of the concentration/time profiles as is evident in Fig. 5a. These sections of the concentration/time profiles are used to locate the onset of reaction[25] and the scatter may affect the accuracy with which this is determined. However, averaging the mass spectra from several identical experiments may reduce the scatter in the data. Such experiments are possible with the DFST and three sets of experiments each consisting of five experiments with identical loading conditions were performed. The loading conditions were chosen to produce conditions corresponding to the low, mid and high temperature points of the DST\TOF-MS experiments. The resulting mass spectra from each set were averaged and the concentration/time profiles extracted from the averaged spectra. Fig. 5a shows the result from a single experiment from the set near the mid point of the temperature range. Fig. 5b shows the concentration/time profile obtained from the average of the five mass spectra from this set. Clearly, the scatter is now much reduced particularly at early times, and this is simply due to the increased S/N and improved peak shapes.

The rate coefficients derived from Fig. 5a and b and the results from averaged spectra at the low and high temperature

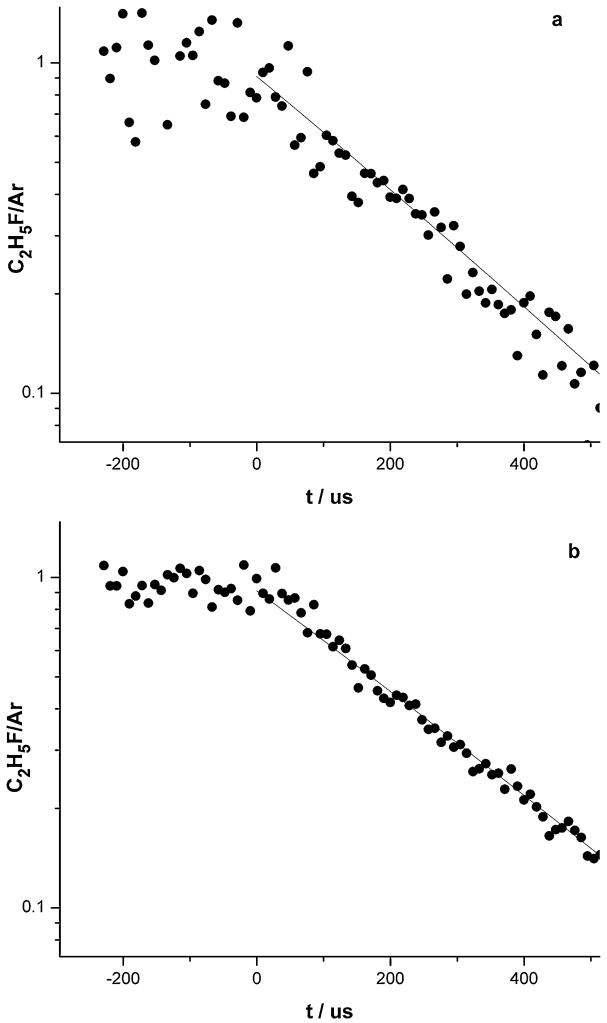

Fig. 5 Concentration/time plots for the dissociation of fluoroethane in DFST/TOF-MS. Solid points represent experimental data and lines represent the results of simulations to extract initial rate coefficients and account for non-isothermal effects. (a) Concentration time profiles for an individual experiment at T_5 = 1397 K, P_5 = 582 Torr; (b) Concentration profile derived from averaged mass spectra from 5 experiments T_5 = 1393 ± 11 K, P_5 = 579 ± 6 Torr.

points are shown in Fig. 6 where they are compared with the results from the DST/TOF-MS experiments (Table 1), single pulse shock tube experiments[16,17] and the results of the current theoretical calculations. As is evident in Fig. 6, the ST/TOF-MS data show strong fall off from k_∞ and a small pressure dependency over the experimental range similar to that observed with DFE.[5] Furthermore, there is excellent agreement between the DFST/TOF-MS results obtained from averaging the mass spectra of several, near identical experiments and the DST/TOF-MS results.

The present QCISD(T)/CBS//QCISD(T)/cc-pvtz predictions for the classical dissociation barrier and dissociation energy are 63.1 and 15.8 kcal mol^{-1}, respectively. With QCISD(T)/cc-pvtz zero point corrections, these values are revised to 58.4 and 10.8 kcal mol^{-1}, respectively. The Q1 diagnostic[43] is 0.022 or lower for each of the stationary points considered here. The low value of this diagnostic suggests that

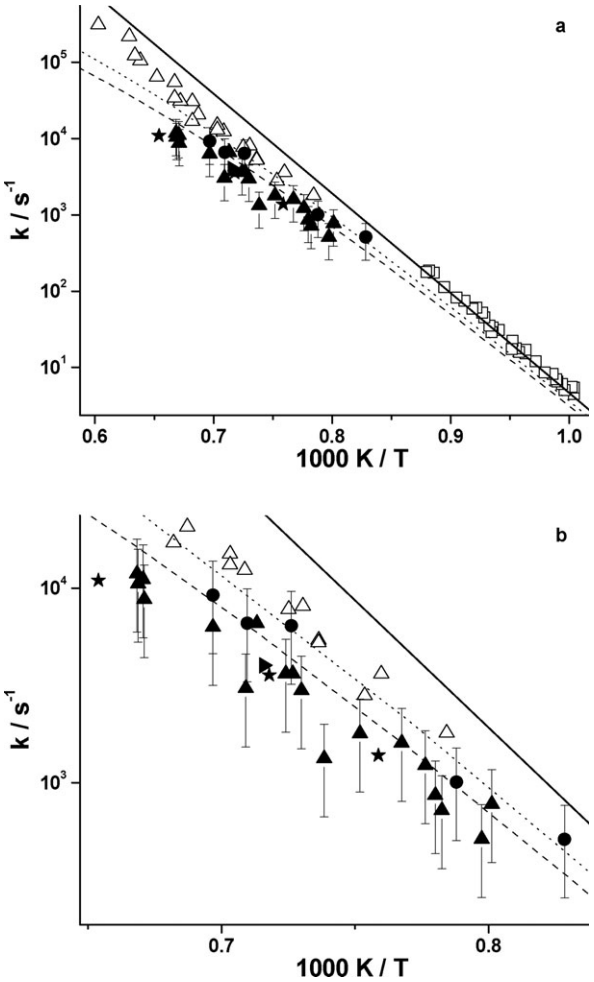

Fig. 6 Arrhenius plot of the ST/TOF-MS results and comparison with the shock tube literature data and the results of the master equation calculations. (a) shows the complete range and (b) is an expanded view of the current work. △ Cadman *et al.*;[17] □ Okada *et al.*;[16] DST experiments: ▲ 500 Torr; ● 1200 Torr. DFST experiments, 500 Torr: ▶ single experiment; ★ average of five mass spectra; Master Equation results: dashed line 500 Torr; dotted line 1200 Torr; solid line k_∞.

there is little multireference character to the wavefunction at any of the stationary points in this dissociation. Thus, these QCISDT(T)/CBS predictions should be quite accurate, *i.e.*, with uncertainties of 1–2 kcal mol^{-1}.

HF elimination from FE has been the subject of a few prior theoretical studies,[9,44–49] although by current standards, none have been at a particularly high level. The highest level previous calculations are the CCSD(T)/6-311++G(d,p) calculations of Hase and coworkers.[49] Their prediction of a zero point corrected reverse reaction barrier of 51.62 kcal mol^{-1} is substantially larger than the present prediction of 47.6 kcal mol^{-1}.

The present *ab initio* VTST predictions for the high pressure limit of the dissociation rate constant are illustrated in Fig. 7 together with the available experimental data.[12–16] The predicted rate exceeds the experimental results for all temperatures, but especially at the lowest temperatures where the discrepancy is about a factor of 2. This suggests that there may be some modest error in the calculated barrier height.

Table 1 Experimental conditions and the corresponding rate coefficients for the thermal unimolecular dissociation of fluoroethane

P_5/Torr	T_5/K	k/s^{-1}
1448	1551	14 400
1543	1409	6599
1273	1269	1005
1110	1514	13 520
1153	1207	511
1326	1377	6399
1262	1435	9183
1176	1491	9993
594	1381	3633
515	1282	862
614	1248	776
604	1330	1791
609	1495	10 540
640	1491	11 100
539	1490	8764
447	1254	514
570	1435	6326
578	1370	2980
563	1278	722
678	1556	12 760
396	1354	1331
508	1496	11 870
608	1410	3057
601	1303	1606
647	1560	14 106
483	1288	1230

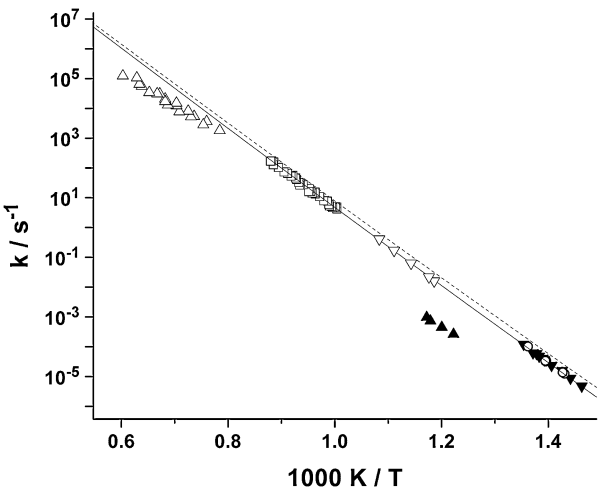

Fig. 7 Comparison of the experimental literature data for FE dissociation and the VTST calculation of k_∞. △ Cadman *et al.*;[17] ▽ Sianesi *et al.*;[14] ▲ Dastoor and Emovoon;[15] ▼ Day and Trotman-Dickenson;[12] ○ Kerr and Timlin;[13] □ Okada *et al.*[16] Solid line E_0 = 59.4 kcal mol^{-1}; dashed line E_0 = 58.4 kcal mol^{-1}.

Raising the barrier by 1 kcal mol^{-1} yields predictions that are in quantitative agreement with almost all of the experimental results. The data of Dastoor *et al.*[15] are clearly discordant with the other experimental data, while the data of Cadman *et al.*[17] are likely not in the high pressure limit. Such a revision of the barrier height is well within the uncertainties of the quantum chemical predictions, although we should note that the discrepancies may also be indicative of other errors in the calculations such as the limited treatments of anharmonic and tunneling effects. The above considerations are also in

accord with a slightly higher $\Delta H_{f,298} = -66.5$ kcal mol^{-1} [9] than the literature values of -65.8 kcal mol^{-1} [8] and -65.1 kcal mol^{-1} for FE.[10] The small change in $\Delta H_{f,298}$ has negligible effect on the extracted rate coefficients and calculated reaction conditions.

The theoretical predictions for the pressure dependent rate coefficients illustrated in Fig. 6 were obtained from master equation simulations. The illustrated results employed an average energy transfer per downward collision, $\langle \Delta E \rangle_{down}$, of 150 $(T/298)^n$ cm^{-1}, with $n = 0.4$. This value for n, which correlates with a $\langle \Delta E \rangle_{down}$ of 280 cm^{-1} at 1400 K, yields good agreement with experiment. A value of 0.9 for n, or $\langle \Delta E \rangle_{down}$ of 600 cm^{-1} at 1400 K, is more typical,[40] but yields an overprediction of the experimental data by about 70%. The somewhat smaller than normal value for $\langle \Delta E \rangle_{down}$ is necessary to capture the curvature of the data.

Using the theoretical parameters of Table 2, the rate coefficients were calculated for a wide range of pressures and temperatures. The results are compiled in Table 3 along with k_∞. As is evident in Fig. 6 and 7, the agreement between the theory and the experiments is excellent, and to within experimental uncertainty the master equation results and experimental data show the same small pressure dependency. These results are consistent with those found in DFE[5] where the fall off and pressure dependence could be simulated with a standard RRKM model and those from ethane[6] where a regular RRKM model also simulated the data well. Thus for the sequence H_3CCF_3, H_3CCHF_2, H_3CCH_2F, H_3CCH_3 only TFE displays apparent non-RRKM behavior and no further conclusions regarding the source of this can be drawn from the current work Vibrational relaxation is very fast in DFE and FE and using ST/LS double relaxation and incubation can be observed in TFE and ethane, although the incubation periods are much shorter in ethane than TFE.

Table 2 Molecular and transition state properties used in the Master Equation calculations for 1,2 elimination of HF from FE

Molecular vibrational frequencies/cm^{-1}	253, 410, 814, 878, 1045, 1118, 1181, 1229, 1398, 1422, 1481, 1497, 1515, 3033, 3041, 3081, 3098, 3115
Transition state vibrational frequencies/cm^{-1}	445, 455, 501, 819, 871, 943, 1104, 1233, 1270, 1287, 1465, 1543, 1630, 3128, 3165, 3215, 3263
Moments of inertia/ 10^{-40} g cm^2	
Molecular	103.25, 90.65, 23.21
Transition state	116.58, 96.89, 31.04
Reaction path degeneracy	3
Barrier (E_0)/kcal mol^{-1}	59.4
$\langle \Delta E \rangle_{down}$/cm^{-1}	150 $(T/298\ \mathrm{K})^{0.4}$
L–J collision parameters	
Collision diameters/Å :	C_2H_5F: 4.4, Ne: 2.8
Potential well depth (ε/k)/K :	C_2H_5F: 300, Ne: 36

Table 3 Calculated rate coefficient parameters[a] $k(T = 900$–2000 K, $P)$ for $C_2H_5F = C_2H_4 + HF$

P/Torr	Log A	n	E_a
1	45.25	−10.493	275
10	45.25	−10.147	285
100	45.25	−9.799	297
500	45.25	−9.563	308
1200	45.25	−9.441	313
10 000	45.25	−9.162	327
∞	13.74	—	250

[a] The rate parameters are given in the form: $k(T) = AT^n \exp(-E_a/RT)$ in units of s^{-1}, mol, kJ, K.

Acknowledgements

This work was supported by the Office of Basic Energy Sciences, Division of Chemical Sciences, Geosciences, and Biosciences, US Department of Energy, under contract DE-AC02-06CH11357 (Argonne) and DE-FE85ER13384 (UIC).

References

1 J. H. Kiefer, C. Katopodis, S. Santhanam, N. K. Srinivasan and R. S. Tranter, *J. Phys. Chem. A*, 2004, **108**, 2443–2405.
2 B. R Giri and R. S. Tranter, *J. Phys. Chem. A*, 2007, **111**, 1585–1592.
3 J. R. Barker, P. J. Stimac, K. D. King and D. M. Leitner, *J. Phys. Chem. A*, 2006, **110**, 2944–2954.
4 P. J. Stimac and J. R. Barker, *J. Phys. Chem. A*, 2006, **110**, 6851–6859.
5 H. Xu, J. H. Kiefer, R. Sivaramakrishnan, B. R. Giri and R. S. Tranter, *Phys. Chem. Chem. Phys.*, 2007, **9**, 4164–4176.
6 J. H. Kiefer, S. Santhanam, N. K. Srinivasan, R. S. Tranter, S. J. Klippenstein and M. A. Oehlschlaeger, *Proc. Combust. Inst.*, 2005, **30**, 1129–1135.
7 J. H. Kiefer, in *Shock Waves in Chemistry*, ed. A. Lifshitz, Marcel Dekker, New York, 1981, pp. 219–279.
8 A. Burcat and B. Ruscic, *"Third Millennium Ideal Gas and Condensed Phase Thermochemical Database for Combustion with updates from Active Thermochemical Tables ANL-05/20 and TAE 960"*, Technion-IIT, Aerospace Engineering and Argonne National Laboratory Chemistry Division, September 2005.
9 B. L. Kormos, J. F. Liebman and C. J. Cramer, *J. Phys. Org. Chem.*, 2004, **17**, 656–664.
10 M. R. Zachariah, P. R. Westmoreland, D. R. Burgess, Jr, W. Tsang and C. F. Melius, *J. Phys. Chem.*, 1996, **100**, 8737–8747.
11 S. S. Chen, A. S. Rodgers, J. Chao, R. C. Wilhoit and B. J. Zwolinski, *J. Phys. Chem. Ref. Data*, 1975, **4**, 441.
12 M. Day and A. F. Trotman-Dickenson, *J. Chem. Soc. A*, 1969, 233–235.
13 J. A. Kerr and D. M. Timlin, *Int. J. Chem. Kinet.*, 1971, **3**, 427–441.
14 D. Sianesi, G. Nelli and R. Fontanelli, *Chim. Ind. (Milan)*, 1968, **50**, 619–627.
15 P. N. Dastoor and E. U. Emovon, *J. Chem. Soc., Faraday Trans. 1*, 1972, **68**, 2098–2102.
16 K. Okada, E. Tschuikow-Roux and P. J. Evans, *J. Phys. Chem.*, 1980, **84**, 467–471.
17 P. Cadman, M. Day and A. F. Trotmann-Dickenson, *J. Chem. Soc. A*, 1970, 2498–2503.
18 W. Tsang, *Int. J. Chem. Kinet.*, 1973, **5**, 643–649.
19 J. H. Kiefer and A. C. Manson, *Rev. Sci. Instrum.*, 1981, **52**, 1392–1396.
20 N. K. Srinivasan, J. H. Kiefer and R. S. Tranter, *J. Phys. Chem. A*, 2003, **107**, 1532–1539.
21 S. Santhanam, J. H. Kiefer, R. S. Tranter and N. K. Srinivasan, *Int. J. Chem. Kinet.*, 2003, **35**, 381–390.
22 J. H. Kiefer, S. S. Kumaran and S. Sundaram, *J. Chem. Phys.*, 1993, **99**, 3531–3541.
23 J. Grange, G. Albiser and H. Fousse, *Cah. Phys.*, 1962, **137**, 35.
24 W. C. Gardiner, Jr, Y. Hidaka and T. Tanzawa, *Combust. Flame*, 1981, **40**, 213–219.
25 R. S. Tranter, B. R. Giri and J. H. Kiefer, *Rev. Sci. Instrum.*, 2007, **78**, 034101.
26 R. S. Tranter and B. R. Giri, *Rev. Sci. Instrum.*, in press, AIP 028809RSI.
27 A. D. Becke, *J. Chem. Phys.*, 1993, **98**, 5648–5652.

28 W. J. Hehre, L. Radom, J. A. Pople and P. v. R. Schleyer, Ab initio *Molecular Orbital Theory*, Wiley, New York, 1987.
29 P. Celani and H.-J. Werner, *J. Chem. Phys.*, 2000, **112**, 5546–5557.
30 T. H. Dunning, Jr, *J. Chem. Phys.*, 1989, **90**, 1007–1023; R. A. Kendall, T. H. Dunning, Jr and R. J. Harrison, *J. Chem. Phys.*, 1992, **96**, 6796–6806; D. E. Woon and T. H. Dunning, Jr, *J. Chem. Phys.*, 1993, **98**, 1371.
31 L. A. Curtiss, K. Raghavachari, P. C. Redfern, V. Rassolov and J. A. Pople, *J. Chem. Phys.*, 1998, **109**, 7764–7776.
32 M. J. Frisch, G. W. Trucks, H. B. Schlegel, G. E. Scuseria, M. A. Robb, J. R. Cheeseman, V. G. Zakrzewski, G. A. Petersson, J. A. Montgomery, Jr, R. E. Stratmann, J. C. Burant, S. Dapprich, J. M. Millam, A. D. Daniels, K. N. Kudin, M. C. Strain, O. Farkas, J. Tomasi, V. Barone, M. Cossi, R. Cammi, B. Mennucci, C. Pomelli, C. Adamo, S. Clifford, J. Ochterski, G. A. Petersson, P. Y. Ayala, Q. Cui, K. Morokuma, D. K. Malick, A. D. Rabuck, K. Raghavachari, J. B. Foresman, J. Cioslowski, J. V. Ortiz, B. B. Stefanov, G. Liu, A. Liashenko, P. Piskorz, I. Komaroni, R. Gomperts, R. L. Martin, D. J. Fox, T. A. Keith, M. A. Al-Laham, C. Y. Peng, A. Nanayakkara, C. Gonzalez, M. Challacombe, P. M. W. Gill, B. G. Johnson, W. Chen, M. W. Wong, J. L. Andreas, M. Head-Gordon, E. S. Replogle and J. A. Pople, *GAUSSIAN 98*, Gaussian Inc., Pittsburg, PA, 1998.
33 MOLPRO is a package of *ab initio* programs written by H.-J. Werner and P. J. Knowles, with contributions from J. Almlof, R. D. Amos, A. Berning, D. L. Cooper, M. J. O. Deegan, A. J. Dobbyn, F. Eckert, S. T. Elbert, C. Hampel, R. Lindh, A. W. Lloyd, W. Meyer, A. Nicklass, K. Peterson, R. Pitzer, A. J. Stone, P. R. Taylor, M. E. Mura, P. Pulay, M. Schutz, H. Stoll and T. Thorsteinsson, The majority of calculations reported here were done with Version 2002.6.
34 J. P. Senosiain, S. J. Klippenstein and J. A. Miller, *J. Phys. Chem. A*, 2005, **109**, 6045–6055.
35 POLYRATE–version 9.4, J. C. Corchado, Y.-Y. Chuang, P. L. Fast, W.-P. Hu, Y.-P. Liu, G. C. Lynch, K. A. Nguyen, C. F. Jackels, A. Fernandez Ramos, B. A. Ellingson, B. J. Lynch, V. S. Melissas, J. Villà, I. Rossi, E. L. Coitiño, J. Pu, T. V. Albu, R. Steckler, B. C. Garrett, A. D. Isaacson and D. G. Truhlar, University of Minnesota, Minneapolis, 2005.
36 GAUSSRATE–version 9.4, J.C. Corchado, Y.-Y. Chuang, E. L. Coitiño and D. G. Truhlar, University of Minnesota, Minneapolis, 2006.
37 D.-H. Lu, T. N. Truong, V. S. Melissas, G. C. Lynch, Y.-P. Liu, B. C. Garrett, R. Steckler, A. D. Isaacson, S. N. Rai, G. Hancock, J. G. Lauderdale, T. Joseph and D. G. Truhlar, *Comput. Phys. Commun.*, 1992, **71**, 235.
38 Y.-P. Liu, G. C. Lynch, T. N. Truong, D.-H. Lu and D. G. Truhlar, *J. Am. Chem. Soc.*, 1995, **115**, 2408–2415.
39 J. A. Miller and S. J. Klippenstein, *J. Phys. Chem. A*, 2003, **107**, 2680–2692.
40 J. A. Miller and S. J. Klippenstein, *J. Phys. Chem. A*, 2004, **108**, 8296–8306.
41 J. A. Miller and S. J. Klippenstein, *J. Phys. Chem. A*, 2000, **104**, 2061–2069.
42 NIST Mass Spec Data Center, S. E. Stein, director, *"Mass Spectra"*, in *NIST Chemistry WebBook, NIST Standard Reference Database Number 69*, eds. P. J. Linstrom and W. G. Mallard, National Institute of Standards and Technology, Gaithersburg, MD, 20899, June 2005; available at http://webbook.nist.gov.
43 T. J. Lee, A. P. Rendell and P. R. Taylor, *J. Phys. Chem.*, 1990, **94**, 5463–5468.
44 S. Kato and K. Morokuma, *J. Chem. Phys.*, 1980, **73**, 3900–3914.
45 M. Sola, A. Lledos, M. Duran, J. Bertran and O. N. J. Ventura, *J. Comput. Chem.*, 1990, **11**, 170–180.
46 J. L. Toto, G. O. Pritchard and B. Kirtman, *J. Phys. Chem.*, 1994, **98**, 8359–8370.
47 B. Rajakumar and E. Arunan, *Phys. Chem. Chem. Phys.*, 2003, **5**, 3897–3904.
48 L. Sun and W. L. Hase, *J. Chem. Phys.*, 2004, **121**, 8831–8845.
49 E. Dong, D. W. Setser, W. L. Hase and K. Song, *J. Phys. Chem. A*, 2006, **110**, 1484–1490.